Super-Resolution Techniques Applied to MSTAR Data

Ing. Silvio D'Ercole
AMS – Engineering and Operation
Radar analysis group
Via Tiburtina Km 12,4
00131 Roma
Italia

sdercole@amsjv.it

ABSTRACT

This paper has been produced in the frame of research group for Automatic Target Recognition (ATR), NATO SET 053 TG 29. One of the biggest challenges for automatic target recognition (ATR) methods is the accurate and efficient extraction of features from synthetic aperture radar (SAR) images. The aim of this work is to evaluate the recognition-oriented properties for 2D modified covariance Super-Resolution technique[1]. Recognition-oriented properties in order to enhance features in the scene that are important for recognition purposes. Performances of the technique are evaluated in this paper by testing robustness of preserving and enhancing features extraction. Results indicate that 2D modified covariance Super-Resolution technique formation method provides images with higher resolution of scatterers, and better separability of different regions as compared to conventional SAR images.

1.0 INTRODUCTION

In order to exploit an automatic recognition based on a SAR imagery system, we need to extract certain features from the reconstructed images. These feature extraction can be difficult when based on SAR images formed by conventional Spectral Analysis methods (Specan), such as the two-dimensional matched filter (2D-MF) for reconstruction of the image of the scene sensed from the SAR. A scheme for such a system is represented in Figure 1 (view of the SAR-SPECAN processing scheme) where the 2D dechirping operation is applied to the hologram to remove the frequency modulation introduced on the echo reflected by the single point scatter by the chirped waveform (along the fast-time axis) and by the changing distance from the moving radar receiver (along the slow-time axis). One challenge is that the resolution of the formed images is limited by the SAR system bandwidth. This complicates point scatterer localization, the images suffer from speckle, and in addition this complicates region segmentation for shape-based recognition. The slant range resolution of a SAR transmitting chirp signals of bandwidth B is $\delta_r = c/(2B)$, where c is the speed of light, whereas the cross-range (i.e. azimuth) resolution is approximately (for small observation angles) $\delta_a = \lambda/(2\Delta\theta)$, where λ is the transmission wavelength and $\Delta\theta$ is the angle under which a generic point is observed during the formation of the synthetic aperture. To improve the resolution beyond these limits (usually denoted as Rayleigh limits) it would be necessary to increase the bandwidth of the transmitted signal and the duration of the observation interval. In both cases, besides the associated cost, there are severe constraints on the instrumentation stability and on the knowledge of the relative motion between the radar and the scene, which has to be compensated for to form the synthetic aperture.

Paper presented at the RTO SET Symposium on "Target Identification and Recognition Using RF Systems", held in Oslo, Norway, 11-13 October 2004, and published in RTO-MP-SET-080.

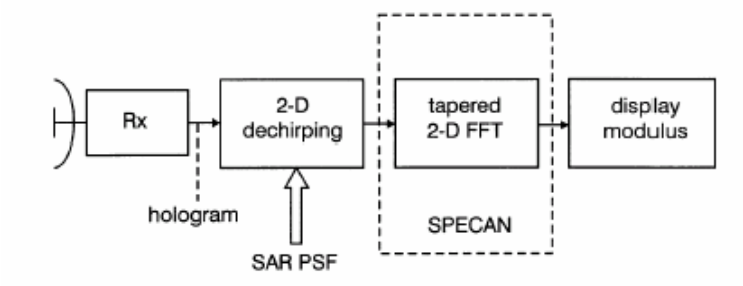

Figure 1. Conventional SAR-SPECAN processing Scheme

Using the 2D-Covariance on SAR images, the resolution can be improved without acting nor on the bandwidth neither on the duration of the observation interval. The improvement of resolution is achieved by finding an adequate parametric model (specifically setting the model orders for the considered 2D AR model) and estimating the parameters of the model.

This method produces images which appear to enhance point-based features (e.g. scatterer locations), and region-based features (e.g. object shapes), such features are important for recognition purposes[2][3][4][5].The AR models are used in this work because they fit well the scattered signal from point reflectors and, to some extent, also the signal from extended scenes. High resolution spectral analysis tools have the advantage, over the conventional FFT, that their spectral resolution improves with increasing SNR. Fourier transform methods obtain a frequency resolution which is constant at about the inverse of the observation time, or, for imaging systems, an angular resolution constant at about the ratio of wavelength to aperture size. The signal backscattered from the scene and captured from SAR has enough signal-to-noise power ratio to exploit for resolution improvement. On the other hand, it is known that the FFT processing is very robust, while super-resolution methods may be sensitive to model errors. A requirement for the application of super-resolution is therefore, that the system accuracy is significantly better than necessary for conventional SAR processing.

In this paper, we use quantitative criteria for evaluating the images produced by this Super-Resolution Spectral Analysis (SR-SPECAN) technique for SAR image formation. Experiments has been done on the Moving and Stationary Target Acquisition and Recognition (MSTAR) public target data set to compare the SAR images formed by the regularized method to conventional images in terms of these quantitative measures. The criteria we use regarding point-based features are target-to-clutter ratio, main-lobe width, peak matching accuracy and average associated peak distance. The metric of peak matching accuracy is particularly useful for testing the super-resolution properties of an image formation technique. The criteria we use for region-based features are segmentation accuracy, and separability of different regions models. The results of this study show that SR-Technique method yields images with higher resolution and better dominant scatterer localization than conventional images, also in considerably reduced amounts of data conditions. In addition when the method is used for region-based extraction, results in enhanced anomaly and speckle suppression in homogeneous regions, and hence, easier-to-segment images.

2.0 SUPER-RESOLUTION OF A SINGLE IMAGE

We now briefly summarize the super-resolution technique developed in [1], [6] and [7]. After having dechirped the SAR hologram, each point scatterer in the SAR scene is encoded into a 2D complex exponential embedded in the white Gaussian noise (WGN), corresponding to the mixture of ground clutter and thermal noise. A conventional spectral analysis (SPECAN), i.e. 2D-FFT, is able to focus at the same time all the point targets in the scene with a resolution equal to the so called Rayleigh limits. Since the dechirped signal backscattered from point targets is made of complex sinusoids with unknown parameters,

super-resolution spectral analysis (SR-SPECAN) techniques can also be applied to extract complex sinusoids embedded in WGN[8]; resolution higher than the conventional SPECAN based on the FFT can be gained. A better discrimination of the point targets in a SAR image is thus obtained by replacing the 2D-FFT with SR-SPECAN techniques. The 2D covariance method[7] estimates the power spectral density of a 2D AR signal via the linear prediction. The AR spectrum depends on the region of support of the processed data. Four regions of supports can be singled out from the grid over which the data are available, namely: the first (upper right hand side), the second (the upper LHS), the third (lower LHS), and the fourth (lower RHS) quarter planes. Thus, four quarter planes (or quadrants) AR spectra are calculated separately; they are combined to form a single unbiased, with circular response (i.e.: with equal resolution along the two orthogonal axes of the data grid), AR spectrum P^{combined} which is derived as follows:

$$\frac{1}{P^{\text{combined}}(f_1,f_2)} = \frac{1}{P^1(f_1,f_2)} + \frac{1}{P^2(f_1,f_2)} + \frac{1}{P^3(f_1,f_2)} + \frac{1}{P^4(f_1,f_2)}$$

where f_1 and f_2 are the spatial frequencies along the two orthogonal axes (in the SAR case, the range and azimuth axes) and P^1, P^2, P^3, and P^4 are the four quarter planes AR spectra. To calculate the single quarter plane AR spectrum the mathematical procedure is the following:

- determine the orders p_1 and p_2, in range and cross-range directions respectively, of the 2D AR model of the data (this step requires a "try and see" procedure and some heuristics; note that the maximum order value is a half of the available data length),
- estimate the 2D AR covariance matrix from the available data,
- write the 2D Yule-Walker equations to find the coefficients of the linear prediction estimator,
- apply the 2D Levinson algorithm to efficiently solve the 2D AR Yule-Walker equations (resort is made to QR decomposition to have a mathematically stable solution).

Because of the computational cost of the technique and of the assumption of a small number of point scatterers against WGN, the above SR-SPECAN technique cannot be applied in one shot to a large SAR image, unlike the 2D-FFT. The practical application of the technique to a SAR image requires the splitting of the image into small sub-images via 2D passband filtering operation, the application of the technique to each sub-image and finally the recombination of the sub-images into the complete super-resolved SAR image.

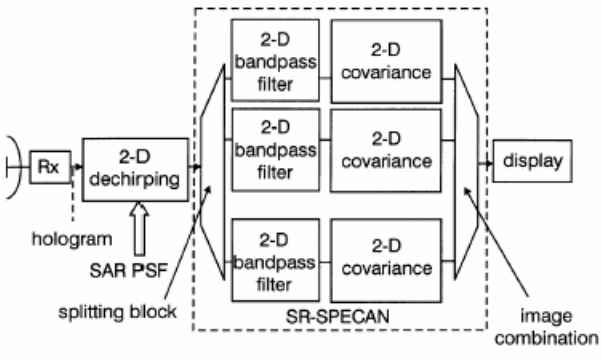

Figure 2. Proposed SR-SPECAN Scheme for SAR images

3.0 FEATURE-BASED CRITERIA FOR EVALUATION OF IMAGE QUALITY

In this section we propose measures for evaluating the quality of images formed by the method outlined in Section 2. Many of these criteria have appeared in the literature before, and they are mostly directed towards images to be used in target recognition tasks.

3.1 Criteria for Point-Enhanced Images

3.1.1 Target-to-clutter ratio

As a measure of accentuation of the target pixels with respect to the background, we will use the target-to-clutter ratio (TCr) in dB, defined as:

$$TCr = 20 \cdot \log_{10}\left(\frac{\max\left(\left|\hat{f}_{i,j}\right|\right)}{\frac{1}{N_c} \cdot \sum_{(i,j)\in\Omega}\left|\hat{f}_{i,j}\right|} \right)$$

Equation 1. Target to Clutter ratio (dB)

where $\hat{f}_{i,j}$ is the reconstructed image, with the pair (i, j) denoting the pixel indices, Ω denotes a clutter patch in the image, and N_c denotes the number of pixels in that patch.

3.1.2 Main-lobe width

As one of the measures of the effective resolution of an image, we will use the 3-dB main-lobe width. To obtain an estimate of the main-lobe width, we concentrate on the target region. In each row and column in the target region of the reconstructed image, we find the first point near the maximum where the reflectivity magnitude is more than 3 dB below the maximum value. We then obtain a better estimate of the 3-dB distance by means of a linear interpolation between pixels. Finally, we average the distances obtained from each row and column in the target region to find an overall estimate of the 3-dB lobe width for a particular image.

3.1.3 Peak matching accuracy

Locations of dominant point scatterers extracted from a target image are important characteristics for recognition. Loss of resolution manifests itself by merging and moving such characteristic points, and this makes the accurate localization of these points in the scene more difficult. Thus, we evaluate the super-resolution properties of our method by measuring how well the dominant scatterers are preserved when we use reduced-resolution data to form the image. For this purpose, we extract the locations of the brightest scatterers from the conventional and the proposed reconstructions using the same reduced-resolution data, and compare these to the "reference" locations of the scatterers. These "reference" positions may be obtained either from the ground truth, in case that is available, or from locations of the scatterers extracted from a higher resolution image otherwise. In order to extract the scatterer locations, we first find the peaks in the reconstructed image. The peaks are taken to be the points where the discrete spatial derivatives of the reflectivity magnitude in both the x and the y directions change sign from positive to negative. Once the peaks are found, we order them based on their magnitude. Once the peaks are extracted, we evaluate how well the coordinates of these peaks match those of the "reference" peaks. This method allows a match declaration between two peaks, if the estimated peak location is within a radius r of the "reference" peak location. Hence it is more powerful than counting only the exact matches, with r used as a variable parameter (r=0 corresponds to counting the exact matches). A one-to-one association of the peaks is made such that the sum of the squared distances between the locations of the "reference" peaks and the corresponding matched peaks from the image is minimized. We can then count the number of matched peaks, to see how well the peaks are preserved.

3.1.4 Average associated peak distance

Another criterion based on peak locations that we will use is the average distance between the two sets of peaks coordinates. To compute this measure, we relax the matching radius r of Sect. 3.1.3, so that each of the peaks from the reconstructed image is matched to a "reference" peak. We then find the average of the distances between these associated peaks.

3.2 Criteria for Region-Enhanced Images

3.2.1 Segmentation accuracy

It is of interest to obtain accurate segmentations of SAR images for effective use of region-based shape features in target recognition. Recently there has been much interest in the development of segmentation algorithms for conventional SAR images. Our region-enhanced images provide easier-to-segment regions as compared to conventional SAR images. We will demonstrate this property by segmenting our reconstructions to target, shadow and background regions by simple adaptive thresholding. To determine the threshold, we find the mean μ and the standard deviation σ of the dB-valued pixel magnitudes in the image. Then, we apply the following decision rule at each pixel:

Equation 2. Segmentation Decision Rule

$$20 \cdot \log_{10}\left(\hat{f}_{i,j}\right) < \mu - c_1 \cdot \sigma \quad \rightarrow \quad \hat{f}_{i,j} \in S$$

$$\mu - c_1 \cdot \sigma \le 20 \cdot \log_{10}\left(\hat{f}_{i,j}\right) < \mu + c_2 \cdot \sigma \quad \rightarrow \quad \hat{f}_{i,j} \in B$$

$$\mu + c_2 \cdot \sigma \le 20 \cdot \log_{10}\left(\hat{f}_{i,j}\right) \quad \rightarrow \quad \hat{f}_{i,j} \in T$$

where T,S,B denote the target, shadow and background regions respectively, and c_1,c_2 are two constants that are fixed beforehand. From a statistical standpoint, it would make more sense to develop a decision metric based on statistics of particular regions. However, our objective here is not to develop the best decision metric, but rather to show that we can obtain reasonable segmentations of the region-enhanced images even by simple suboptimal processing.

4.0 EXPERIMENTAL RESULTS

4.1 Experimental Setup

We use images of T72 (sn 132) tanks, BMP2 (sn c21) tanks, and BTR70 (sn c71) armored personnel carriers from the MSTAR public target data set to evaluate the performance of our reconstructed images in terms of the criteria described in Sect. 3. We use 8 images for each vehicle type, all at 17 depression angle, and evenly spaced in azimuth (approximately 45°) to cover 360°. As we will describe, we also carry out synthetic scene reconstruction experiments to make some evaluations where ground truth is exactly known. In order to apply our algorithm, we need the phase histories (or the range profiles). We obtain the phase histories from the 128 × 128 complex-valued MSTAR images, by undoing the final steps of MSTAR image formation. We first take the 2-D Discrete Fourier Transform (DFT) of the images, then we remove the zero-padding to obtain 100 × 100 phase history samples and next we remove the windowing applied. From the MSTAR file headers, we know that a 35 dB Taylor window has been used. Then we divide the phase history samples by a 2-D Taylor window.

4.2 Super-Resolution Imaging from Full-Resolution Data

We now use the 100 × 100 phase history samples to form Super-Resolved images. We will form interpolated images of a factor 8 over a patch of 64 x 64 centered on target, obtaining a 512 x 512 samples image. Therefore, in order to have conventional SAR SPECAN images of this size for comparison, we first form interpolated 512 × 512 Taylor-windowed Fourier images. Images for both conventional and SR techniques applied for T72, BTR70 and BMP2 are in Figure 3, Figure 4 and Figure 5, the SR images with an AR order determined by a ‘’Try and See’’ procedure, used for both axis, are at the right column. The

dominant scatterer appears to be accentuated as compared to the conventional images at the left column. We do not apply any windowing to the data before processing, since our method is able to suppress sidelobes considerably even with rectangular weighting. However, if desired, the method can be used with windowing. Each image is normalized to their maxima to remove the different scaling factors and finally fused together on a pixel by pixel basis: a non linear fusion law is applied by setting the pixel value of the final image equal to the maximum value of the 25-normalized SR-SPECAN images[9]. This fusion law will yield a final image with the highest number of target scatterers but at the same time will provide the worst background suppression capabilities. See Figure 6 (T72 and BTR70) and Figure 7 (BMP2) for Super-Resolved SPECAN Fused image with maximum technique.

Target Azimuth	T72		BTR70		BMP2	
	Filename	Best Order	Filename	Best Order	Filename	Best Order
0°	HB04025.015	27	HB03973.004	28	HB03893.002	27
45°	HB04034.015	28	HB03982.004	25	HB03901.002	29
90°	HB03852.015	29	HB03988.004	28	HB03909.002	30
135°	HB03802.015	28	HB03995.004	25	HB03917.002	30
180°	HB03809.015	28	HB03938.004	29	HB03926.002	29
225°	HB03935.015	28	HB03947.004	29	HB03875.002	27
270°	HB03824.015	25	HB03956.004	28	HB03876.002	28
315°	HB04016.015	28	HB03964.004	29	HB03884.002	25

Table 1. Best AR order for each 64x64 SR-SPECAN image

Best AR order for each SR-SPECAN image target elaboration are described in Table 1, and taking into account that the maximum order value is a half of the data length (32 in this case for a 64x64 available data), it is clear to see that high AR values (from 25 to 30) are preferred in order to enhance Super-Resolution capabilities.

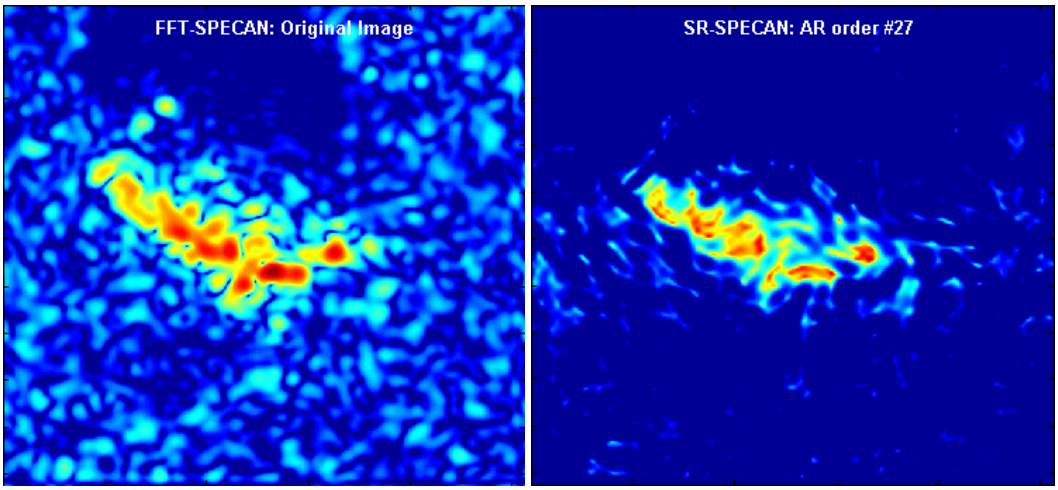

Figure 3. Tank T72 (315° azimuth angle) Left: Specan, Right: SR-Specan with AR order 27 for both axis.

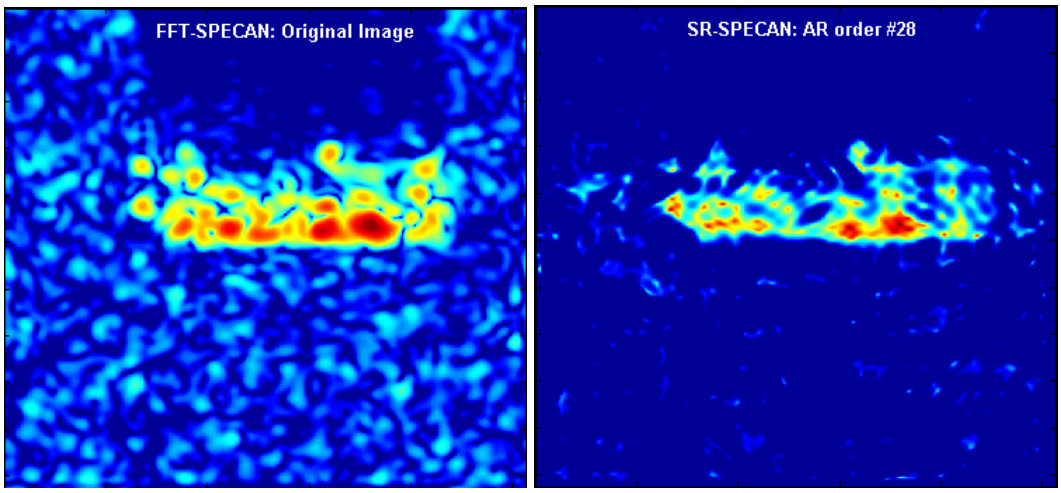

Figure 4. BTR70 (90° azimuth angle) Left: Specan, Right: SR-Specan with AR order 28.

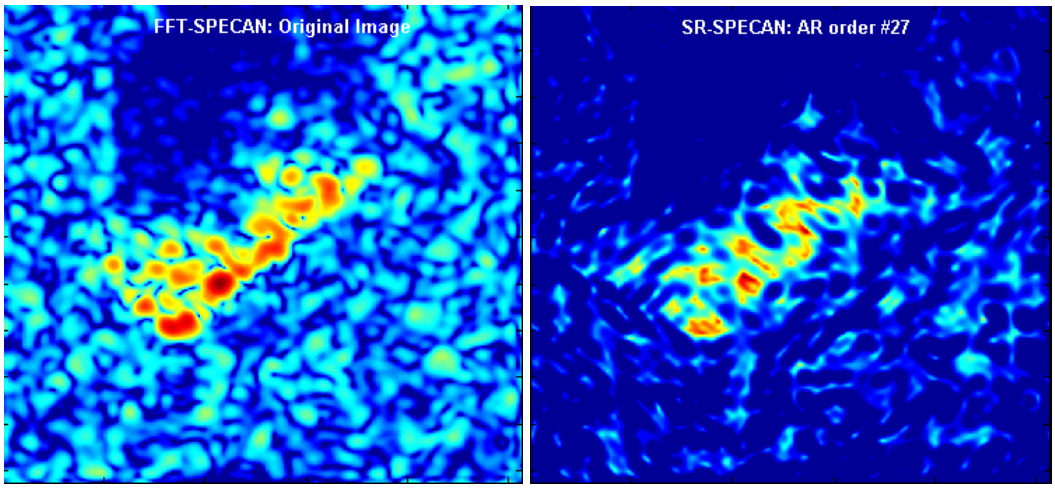

Figure 5. BMP2 (225° azimuth angle) Left: Specan, Right: SR-Specan with AR order 27.

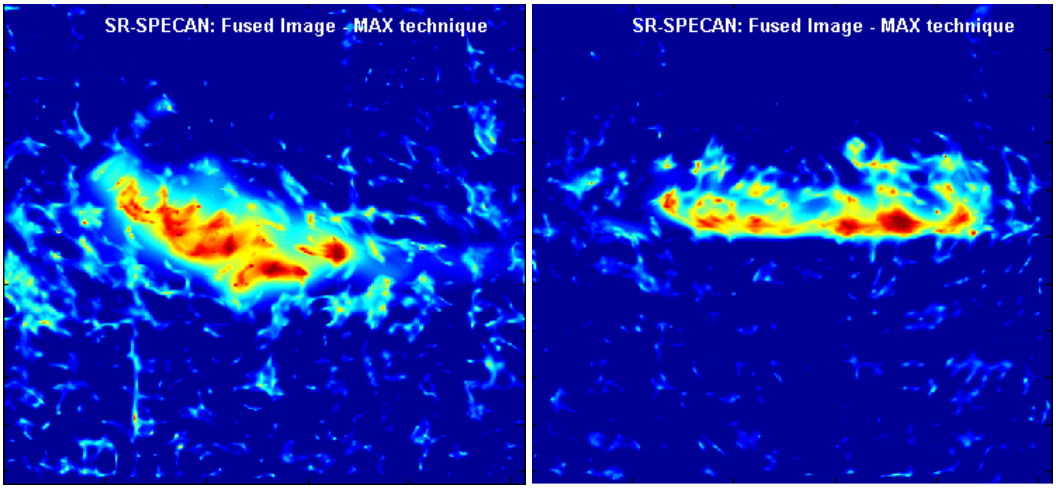

Figure 6. Super-Resolved SPECAN Fused image with MAX technique. Left: Tank T72 (315° azimuth angle) Right: BTR70 (90° azimuth angle)

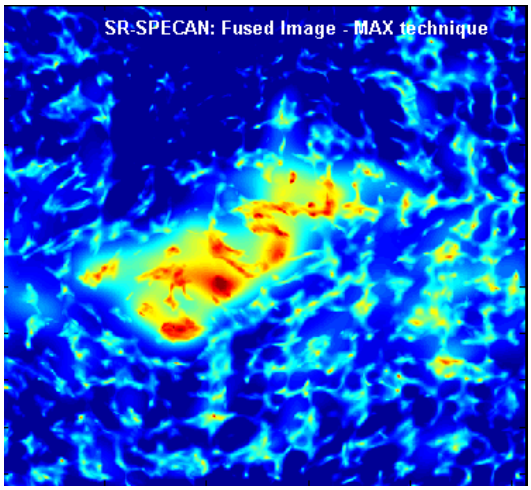

Figure 7. Super-Resolved SPECAN Fused image with MAX technique. BMP2 (225° azimuth angle)

4.2.1 Target-to-clutter ratio

We will quantify the enhancement of the target pixels in the full-resolution data reconstructions by means of their target-to-clutter ratio. We compute the target-to-clutter ratio (TCr(dB)) as defined in Equation 1, by using the bottom 20 rows (2000 pixels) of the reconstructed 100x100 images as the clutter region. Final TCr value is the average over the AR orders SR-SPECAN processing, the AR-values are from 7 to 31. Figure 8, Figure 9 Figure 10 shows the TCr values versus the AR orders for T72, BTR70 and BMP2 respectively, evaluated with an azimuth target angle of 270°. This region is big enough to give a reliable estimate of the mean reflectivity magnitude, and is safe to use, since target and shadow appear to be located outside this region for the entire data set. Table 2 shows the average target-to-clutter ratio achieved by the conventional and the proposed methods over the 8 reconstructed target azimuth variation images for each target type. Last row represent the mean value expressed in dB of the linear TCr evaluated for each azimuth angle. These results indicate a clear improvement of the target-to-clutter ratio by our proposed image formation method.

Target Azimuth	**T72**		**BTR70**		**BMP2**	
	SR	*Conventional*	*SR*	*Conventional*	*SR*	*Conventional*
0°	47.0011	32.1083	54.0255	36.4485	69.3866	42.2303
45°	43.2853	29.2631	34.9206	23.1271	43.912	31.1764
90°	55.2862	35.5263	56.7158	34.2177	64.8596	41.9121
135°	66.1575	41.3393	39.4638	25.3764	42.2591	28.8165
180°	56.4607	36.0822	68.8944	45.3622	55.8789	37.3171
225°	54.6906	36.94	38.7378	27.4282	42.489	30.129
270°	58.4797	36.0718	58.2052	32.8596	61.0104	35.2174
315°	48.633	33.61199	36.9852	22.0673	43.5977	30.581
Average	***56.4244***	***35.7657***	***56.0766***	***34.3262***	***58.8564***	***36.1692***

Table 2. Average target-to-clutter ratios of SR-SPECAN and Conventional processing

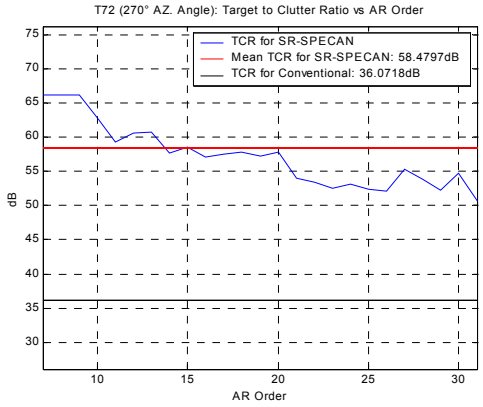

Figure 8. Target to Clutter Ratio vs AR order for T72 (270°)

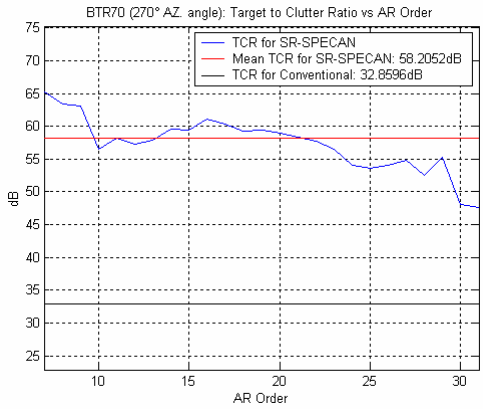

Figure 9. Target to Clutter Ratio vs AR order for BTR70 (270°)

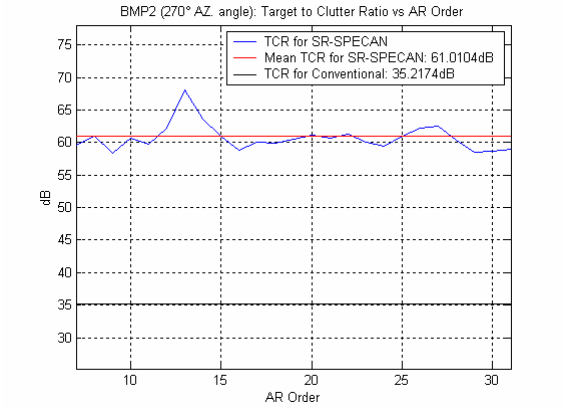

Figure 10. Target to Clutter Ratio vs AR order for BMP2 (270°)

4.3 Point-Enhanced Super-Resolution Imaging from Reduced-Resolution Data

In this section, we carry out experiments on two sets of data: those from the actual MSTAR images, and those from synthetic point scatterer scenes constructed using the MSTAR images. The reason for using synthetic examples is to demonstrate the super-resolution properties of our method in a situation where the ground truth is exactly known. We will present the main-lobe width results for the actual MSTAR reconstructions only. We will present the peak matching accuracy and the average associated peak distance results for both actual and synthetic images. We do not present the target-to-clutter ratio results in this section, since they are very similar to the full-resolution target-to-clutter ratio results. For experiments on actual MSTAR data, we form images from a 50 × 50 subset of the 100 × 100 phase history samples previously used. This results in a two times resolution loss in the range and cross-range directions. All the images we will form in this section are composed of interpolated 512 × 512 from the 50 × 50 subset. The left image in Figure 11 shows Taylor weighted Fourier images from the tank T72 (315° target azimuth) reduced-resolution data. The resolution loss in these images is evident when they are compared to their high-resolution counterparts in left image of Figure 3. We now form Super-Resolved image with an AR order of 20 for each axes, samples of which are shown in the right of Figure 11.

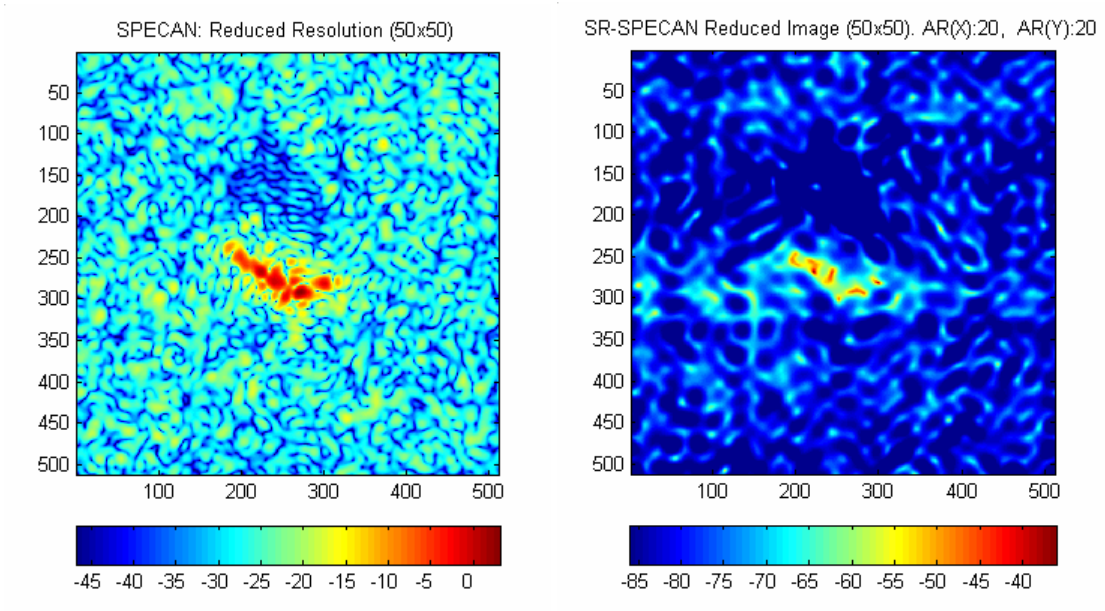

Figure 11. Sample images reconstructed from reduced-resolution (50 × 50) data. Left: conventional SPECAN. Right: proposed SR-SPECAN

The main-lobe-width, as described in Equation 1, of conventional reduced resolution image (50x50) is equal to 0.2650m and 0.0614m for the SR-SPECAN method, a ratio factor of 4.3159 is reached, enhancing the width-lobe-reducing capabilities of our proposed method. We now consider the synthetic examples. To generate synthetic scenes we find the 13 peaks with the largest magnitude in the tank T72 (315° target azimuth) 128×128 Taylor-windowed Fourier images, and form a synthetic scene by placing simulated point-scatterers at the locations of these peaks, with the original complex reflectivity, and zeros in the rest of the scene. An example pixel-plot of the magnitude of such a synthetic scene is shown in Figure 12. We then generate simulated phase histories from this scene. The reconstructed conventional Taylor-windowed image from 64×64 phase history contour plot is shown at the left side, down row, of Figure 13. The average main lobe width is 0.225m, in this case loss of resolution is easy to observe. The corresponding Super-Resolution image produced by our method is shown at the right side, with an average main lobe width of 0.0812m, and we can visually observe that most of the scatterers that were merged by the conventional reconstruction are now resolved.

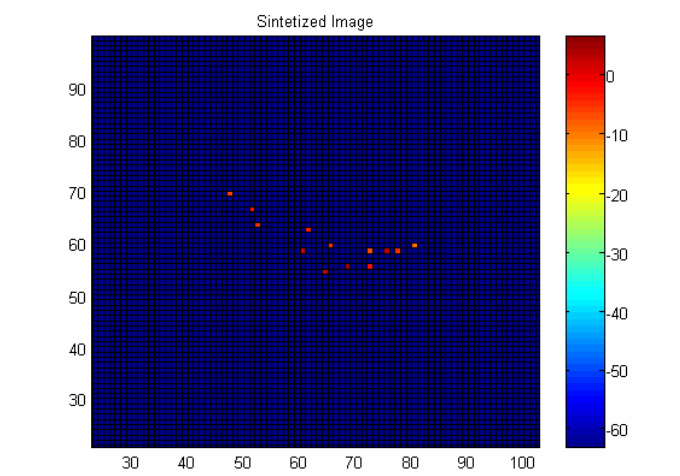

Figure 12. Thirteen points synthetic image from T72 (315° azimuth angle)

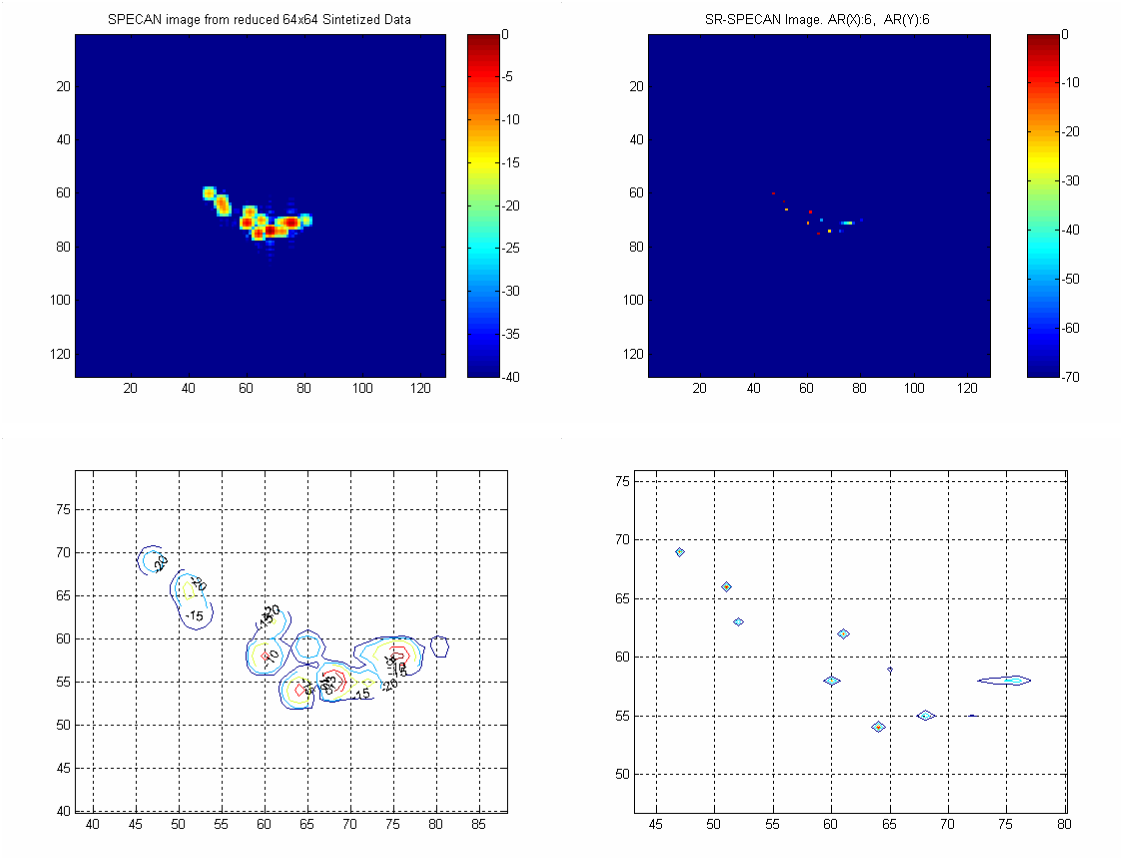

Figure 13. Synthetic T72 image reconstruction from reduced-resolution data. Up: ground truth. Down: results from 64x64 data, left: SPECAN, right SR-SPECAN

4.3.1 Main-lobe width

We compute the average 3-dB main-lobe width (AMLW) as described in Sect. 3.1.2 for all the 8-azimuth-direction reconstructed MSTAR scenes of each target. The AMLW for the proposed method has been calculated as the mean AMLW over the super-resolved images starting from AR order 7, ending to 31 (see Figure 14 for an example on tank T72 with 270° target azimuth angle). The results in Table 3 show that our proposed scheme is able to reduce the lobe width considerably. To put these numbers in perspective, note that the resolution supported by the data is 0.6 m in this experiment. In last row of Table 3 we report the Improvement factor calculated as the ratio of mean AMLW for conventional and proposed method.

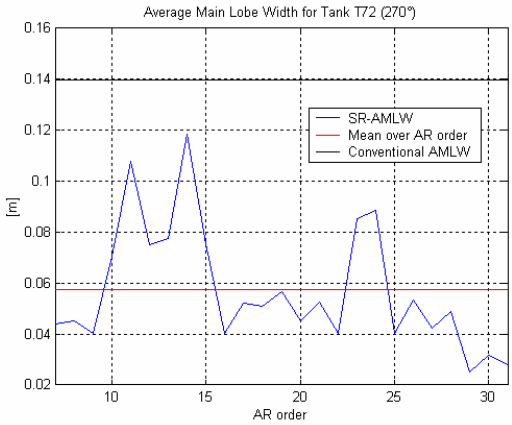

Figure 14. AMLW for T72 image vs AR order

Target Azimuth	**T72**		**BTR70**		**BMP2**	
	SR	*Conventional*	*SR*	*Conventional*	*SR*	*Conventional*
0°	0.1345	0.2144	0.0633	0.1626	0.1368	0.2803
45°	0.0937	0.1889	0.1292	0.1943	0.0817	0.1548
90°	0.0852	0.1803	0.1347	0.2463	0.0835	0.2068
135°	0.0772	0.159	0.1115	0.1745	0.0892	0.2330
180°	0.1412	0.2473	0.1243	0.1962	0.0789	0.1656
225°	0.1337	0.2490	0.0761	0.1582	0.0992	0.1929
270°	0.0574	0.1398	0.0854	0.2780	0.0879	0.3534
315°	0.0892	0.1702	0.0727	0.1874	0.0747	0.1595
Average	***0.1015***	***0.1936***	***0.0997***	***0.1997***	***0.0915***	***0.2183***
I Factor	***1.9***		***2***		***2.38***	

Table 3. Average mail-lobe-widths of images for proposed and conventional methods

4.3.2 Peak matching accuracy and average associated peak distance (AAPD)

We now evaluate how the locations of the dominant peaks are preserved in reduced-resolution data situations by the conventional reconstructions and by our point-enhanced images. For the MSTAR examples, we use the locations of the 13 peaks extracted from tank T72 (315° azimuth angle) Taylor-windowed synthetic image reconstructed from full data (

Figure 12). Figure 15 provides a visual comparison of the peak locating accuracy of the reconstructions from 64×64 data, comparing peaks extracted from our images with those from the conventional ones. The circles indicate the "reference" locations of the 13 dominant scatterers, and the plus signs indicate the peaks extracted from the reconstructed reduced-resolution images. Left side contains results for the conventional images, while right side contains those for the SR images. The clear observation we can make out of these results is that, since conventional image formation causes peaks to merge, some of the peaks in the target area are lost, and peaks outside this area may become dominant. We will now evaluate the peak matching accuracy of our method by using the criterion described in Sect. 3.1.3. In Figure 17, Figure 18, Figure 19, we plot the average number of peak matches for the images formed by the conventional and the proposed methods as a function of the radius r within which a match declaration is allowed, respectively for T72, BTR70, and BMP2. The peak matching accuracy of our images appear to be higher than that of the conventional images. Note that our analysis is based on finding peaks all around the scene. Alternatively, the search for peaks can be done in a pre-determined target region only. The improved accuracy provided by our method is easy to observe in these plots.

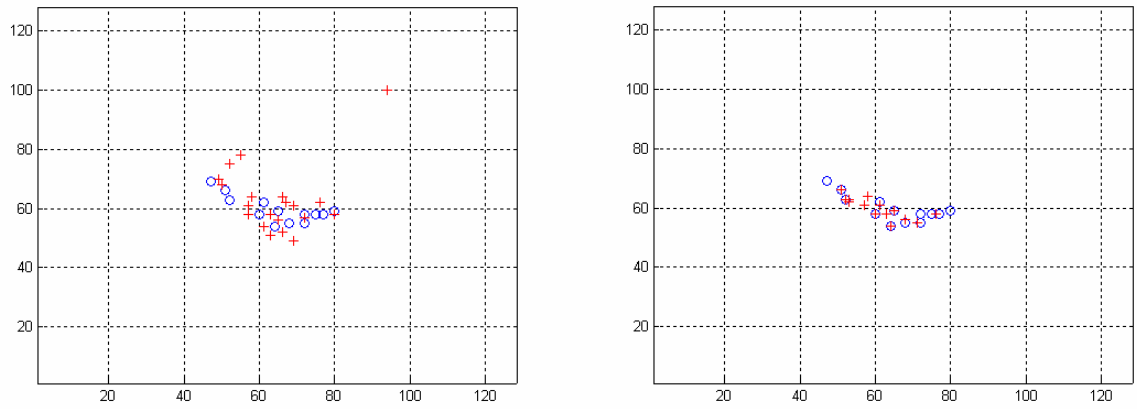

Figure 15. Sample peak extraction results for the synthetic reduced 64x64 T72 scenes. Circles indicate the scatterer locations in the synthetic scene. Plus signs indicate peaks extracted from the reconstructed images. Left: Conventional. Right: Proposed SR method.

The average distance between the true synthesized 13 peaks and the 13 peaks extracted from the reconstructed images as described in Sect. 3.1.4 is 0.46m for conventional method and 0.088m for proposed SR-SPECAN. These results indicate a clear reduction in peak distances by our method. Now we evaluate peak matching accuracy of both conventional and proposed method over reduced resolution method. Reduced images are formed from 64×64 reduced synthetic 256×256 image (loss resolution factor 4). A Taylor-window is applied for conventional method. Table 4, Table 5 and Table 6 show such performance results for each target type. It is clear to see how peak matching probabilities of proposed SR-SPECAN method is higher than that of conventional one with a reduced averaged associated peak distance. The AR order chosen for both axes in SR methods is 3. Figure 16 shows one matching example for BTR70 target, with relative average number of peak matches curves for the synthetic scene as a function of the radius of match declaration.

Target	**T72**			
	SR		*Conventional*	
Azimuth	Matches	AAPD(m)	Matches	AAPD(m)
0°	12/12	0	6/12	0.0167
45°	11/11	0	9/11	0.0111
90°	12/12	0	8/12	0.0530
135°	14/14	0	7/14	0.0429
180°	12/15	0.0167	5/15	0.0766
225°	14/14	0	6/14	0.0471
270°	19/21	0.1972	10/21	0.0883
315°	11/11	0	5/11	0.0483
Average	***96.3%***	***0.0267***	***52%***	***0.048***

Table 4. Peak matching accuracy and average associated peak distance (AAPD) performance for T72 data

Target Azimuth	**BTR70**			
	SR		*Conventional*	
	Matches	AAPD(m)	Matches	AAPD(m)
0°	16/19	0.1207	7/19	0.0866
45°	12/12	0	8/12	0.0405
90°	18/18	0.1128	10/18	0.0200
135°	12/12	0	4/12	0.1377
180°	10/17	0.0200	4/17	0.0854
225°	15/15	0	7/15	0.1178
270°	14/14	0.0706	5/14	0.0400
315°	10/10	0	8/10	0.1361
Average	***92.8%***	***0.0405***	***47.3%***	***0.0830***

Table 5. Peak matching accuracy and average associated peak distance (AAPD) performance for BTR70 data

Target Azimuth	**BMP2**			
	SR		*Conventional*	
	Matches	AAPD(m)	Matches	AAPD(m)
0°	9/9	0	4/9	0.0604
45°	8/8	0	6/8	0
90°	12/23	0.1369	6/23	0.1177
135°	8/8	0	7/8	0
180°	18/18	0.1063	8/18	0.0427
225°	11/11	0	8/11	0.0375
270°	9/19	0.0824	4/19	0.1104
315°	10/10	0	7/10	0.0143
Average	***87.5%***	***0.0407***	***55.1%***	***0.0479***

Table 6. Peak matching accuracy and average associated peak distance (AAPD) performance for BMP2 data

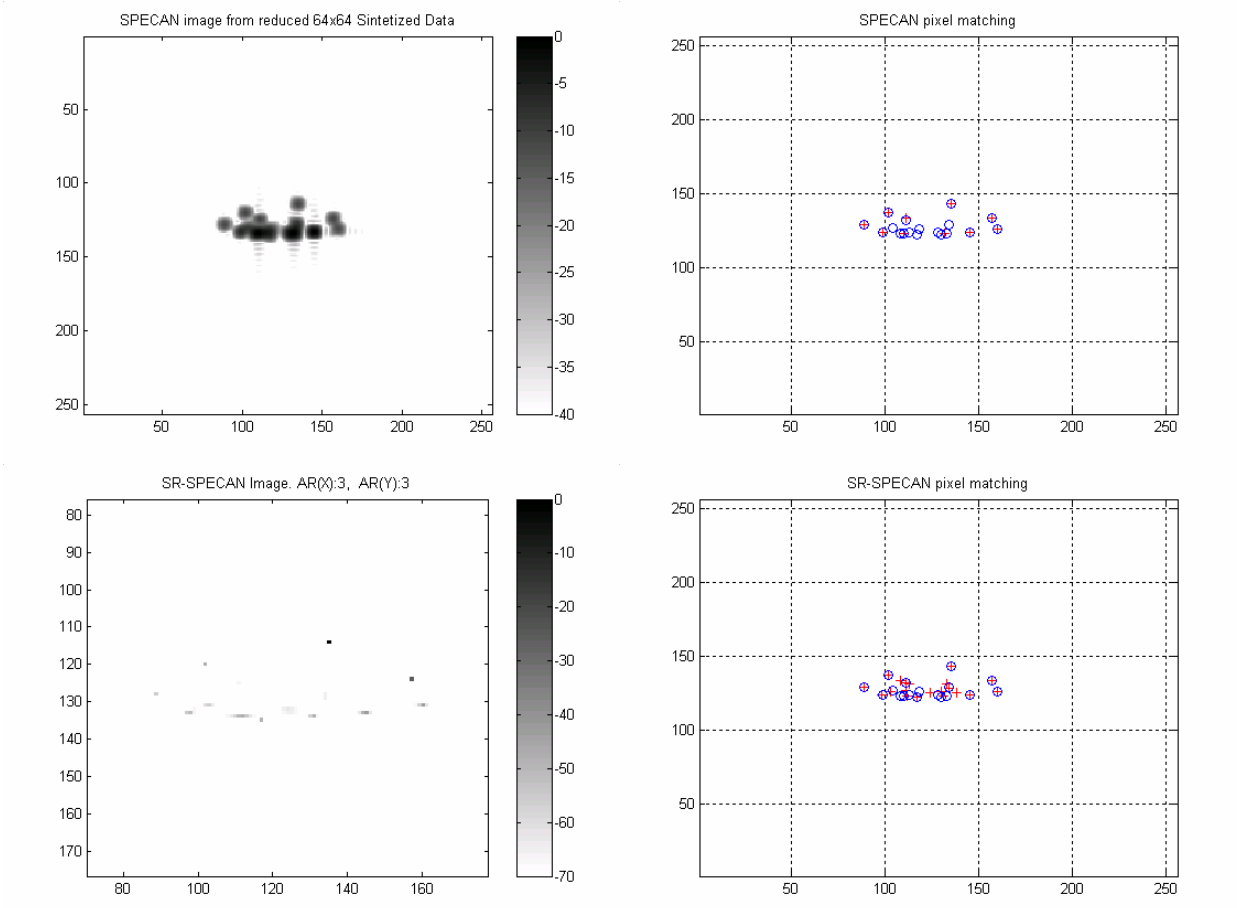

Figure 16. BTR70 (90°) Left column: reconstructed image from reduced 64x64 data. Right: pixel matching image. Top: Conventional. Bottom: Proposed method.

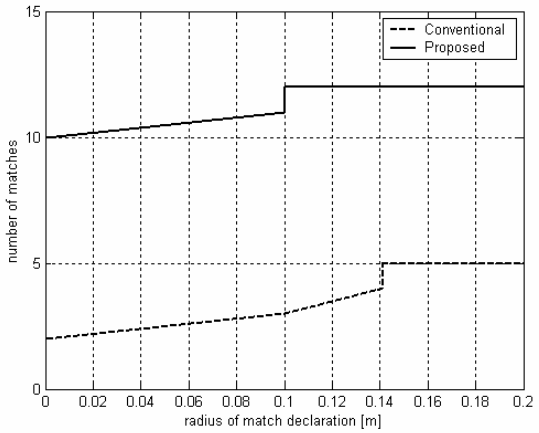

Figure 17. Average number of peak matches for the synthetic T72 (180°) scene as a function of the radius of match declaration r

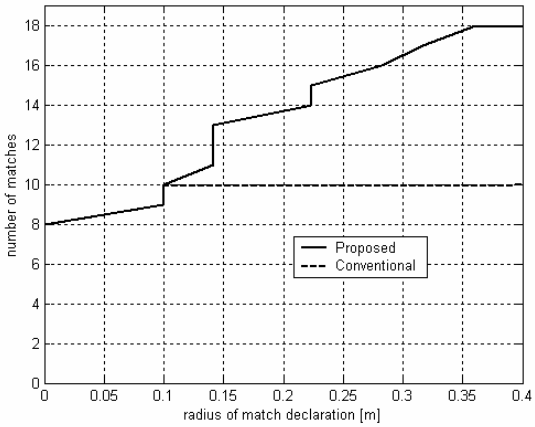

Figure 18. Average number of peak matches for the synthetic BTR70 (90°) scene as a function of the radius of match declaration r

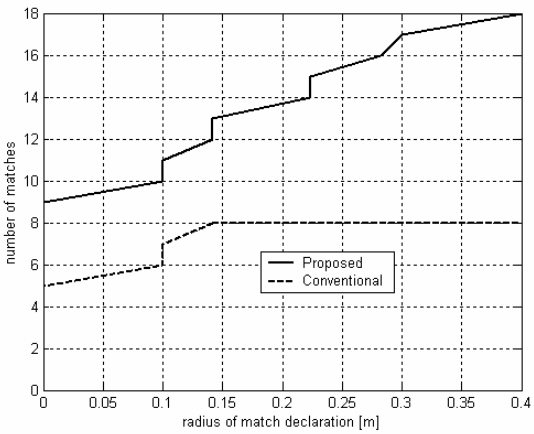

Figure 19. Average number of peak matches for the synthetic BMP2 (180°) scene as a function of the radius of match declaration r

4.4 Region-Enhanced Imaging

We now compare our region-enhanced images with conventional ones in terms of the criteria described in Sect. 3.2.1. Here, we form interpolated images patches (factor 8) from 128 × 128 Taylor-weighted phase history samples. In our proposed SR-method, we use an AR order equal to 20 for each target type and both axis, we will see that low AR values are preferred in order to enhance regions segmentation.

4.4.2 Segmentation accuracy

We segment our region-enhanced images by simple adaptive thresholding as described in Sect. 3.2.1, using c_1=1 and c_2=2 for both proposed and conventional method. Pictures from Figure 20 to Figure 22 shows sample reconstructions using the conventional and proposed method for BTR70 target type. In contrast to the conventional images, the SR reconstructions reduce variability in homogeneous regions, while preserving discontinuities at region boundaries. These results show that segmentation is considerably simplified by our reconstruction method. It is clear to see that such thresholding-based segmentation applied to conventional images, produce results dominated by fluctuations in homogeneous regions. We have also discovered that low AR order values are optimum for best segmentation performance.

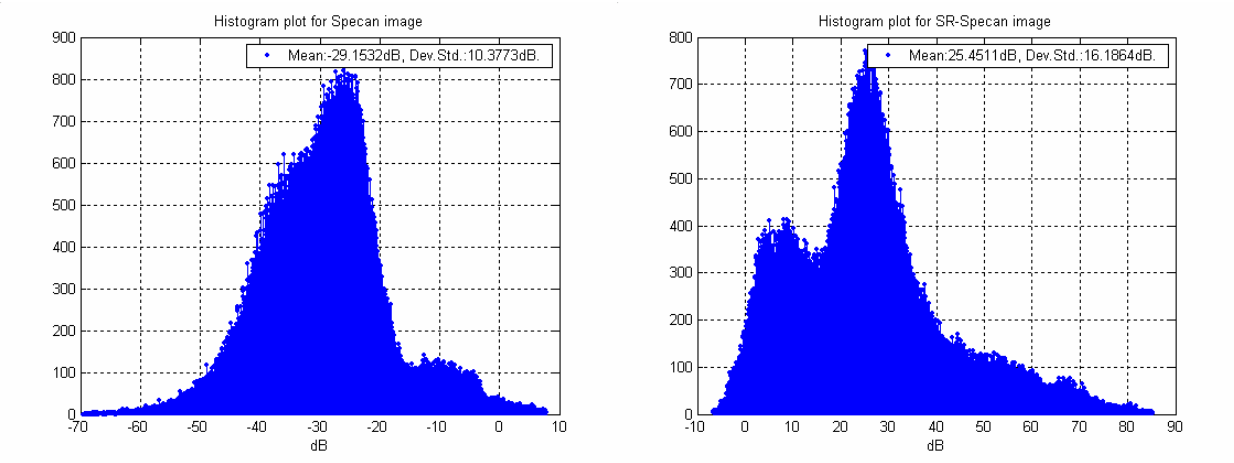

Figure 20. BTR70 (90°). Histogram plot from reconstructed data. Left: Conventional. Rigth: Proposed.

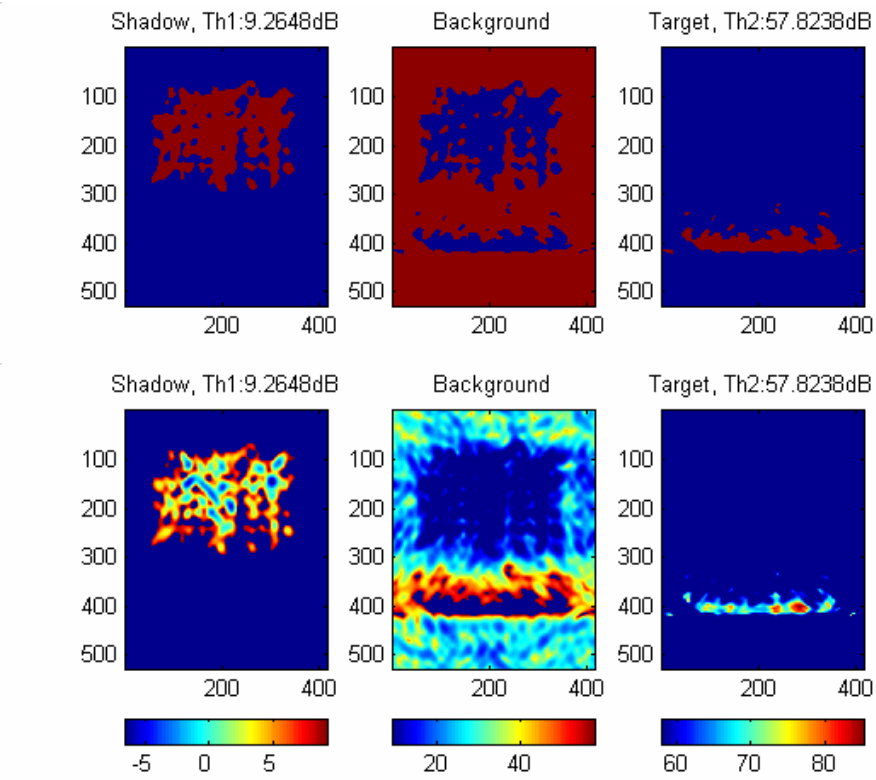

Figure 21. BTR70 (90°). SR-Specan: Results post Image Segmentation. Top row: Binary mask. Bottom row: Results.

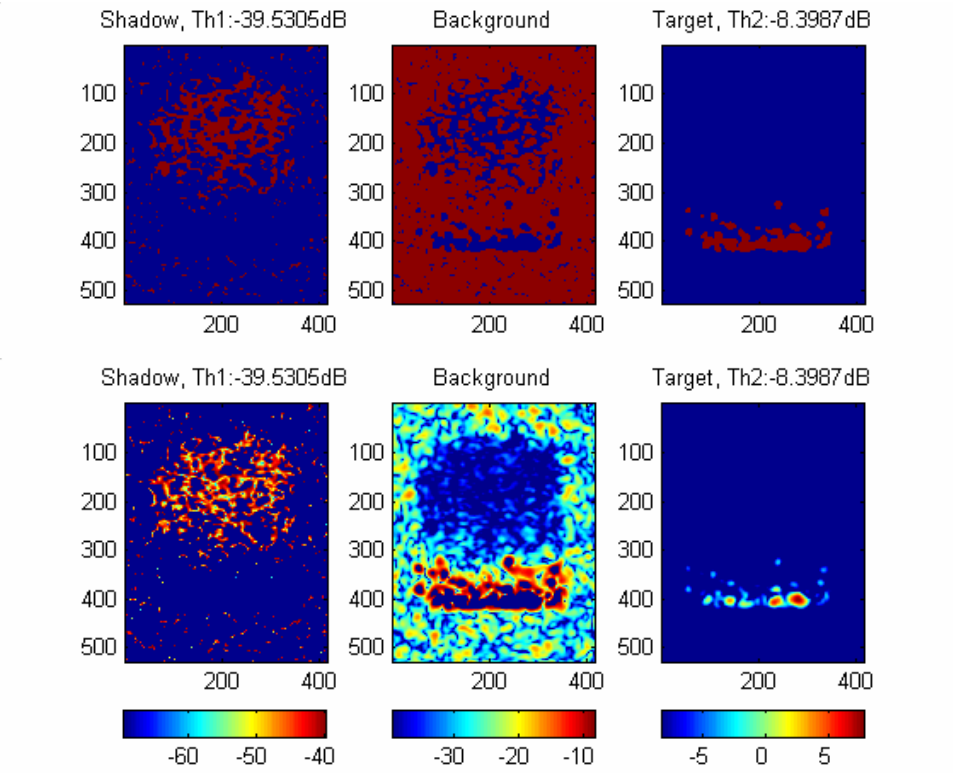

Figure 22. BTR70 (90°). Specan: Results post Image Segmentation. Top row: Binary mask. Bottom row: Results.

5.0 CONCLUSION

We have demonstrated the feature-enhancement properties of Super-Resolution method using 2D modified covariance method through a variety of quantitative criteria. The results indicate that the images produced by this method exhibit super-resolution and improved localization accuracy for dominant scatterers when high AR orders are used, and improved separability for different regions for low AR orders. With these properties, the method seems to have the potential for improving the performance of ATR systems. At the moment polar and multi-frequency data has been used to "combine multi-domain data" with proposed fusion method in order to increase correct classification probabilities. Future work will involve running recognition tests on images produced by this technique, and automatic selection of AR order (Akaike Information Criteria and Minimum description length).

6.0 ACKNOWLEDGMENTS

I personally thank sage colleague Alfonso Farina who let me enter in this NATO research group and helps me in imaging and super-resolution contents too. Debora Pastina (Dept. InfoCom – University of Rome "La Sapienza", via Eudossiana 18, 00184 Rome, Italy) for providing the core of super-resolution algorithm and her patience aid which has been guided me with the use of the software.

7.0 REFERENCES

[1] D.Pastina, A.Farina, J.Gunning, P.Lombardo. "Two-Dimensional super-resolution spectral analysis applied to SAR images". IEE Proc. Radar, Sonar Navigation ,Vol. 145, No. 5, October 1998

[2] B. Bhanu. “Automatic target recognition: state of the art survey”. IEEE Trans. Aerospace and Electronic Systems, AES-22, pp. 364-379, 1986

[3] L.C. Potter, R.L. Moses. “Attributed scattering centers for SAR ATR”. IEEE Trans. Image Processing, 6, pp. 79-91, 1997

[4] G. Jones, B.Bhanu. “Recognition of articulated and occluded objects”. IEEE Trans. Pattern Anaò. Machine Intell., 21, pp.603-613, 1999

[5] J.A. Ratches, C.P. Walters, R.G. Buser. “Aided and automatic target recognition based upon sensory inputs from image forming systems”. IEEE Trans. Patter Anal. Machine Intell., 19, pp. 1004-1019, 1997

[6] S.L.Marple. “A fast algorithm for the two dimensional covariance method of linear prediction”. Proceedings of International conference on Acoustic speech and signal processing, ICASSP 1995, Detroit, MI, pp. 1693-1696.

[7] S.L.Marple: “2D AR algorithm based on the 2D covariance method of linear prediction”, private communication 1994.

[8] S.L.Marple: “Digital Spectral analysis with applications”, Prentice-Hall Inc., 1987.

[9] D.Pastina, A.Farina, P.Daddi, P.Lombardo. “Super-Resolution of polarimetric SAR images of ship targets”. IGARSS 2001